Synchrotron radiation spectra and synchrotron radiation spot shape of runaway electrons in Experimental Advanced Superconducting Tokamak

R. J. Zhou, I. M. Pankratov, L. Q. Hu, M. Xu, and J. H. Yang

Citation: Physics of Plasmas (1994-present) **21**, 063302 (2014); doi: 10.1063/1.4881469
View online: http://dx.doi.org/10.1063/1.4881469
View Table of Contents: http://scitation.aip.org/content/aip/journal/pop/21/6?ver=pdfcov
Published by the AIP Publishing

Synchrotron radiation spectra and synchrotron radiation spot shape of runaway electrons in Experimental Advanced Superconducting Tokamak

R. J. Zhou,[1] I. M. Pankratov,[2] L. Q. Hu,[1] M. Xu,[1] and J. H. Yang[1]
[1]*Institute of Plasma Physics, Chinese Academy of Sciences, Hefei 230031, China*
[2]*Institute of Plasma Physics, NSC "Kharkov Institute of Physics and Technology," Academicheskaya Str.1, 61108 Kharkov, Ukraine*

(Received 17 January 2014; accepted 19 May 2014; published online 2 June 2014)

A detailed analysis of the spectra of synchrotron radiation emitted by runaway electrons, and an analysis of synchrotron radiation spot shapes are presented for EAST runaway cases. Conditions required for the asymptotic expressions of synchrotron radiation spectra to be valid are studied for these EAST parameters. We provide the correct synchrotron radiation spectra in typical EAST discharges, and we show results of calculations of the shape of the synchrotron radiation spots emitted by runaway electrons. These shapes are detected by a visible light camera in EAST. Safety factor $q(r)$, the horizontal displacement of electron drift surfaces with respect to the magnetic surfaces δ_e, pitch angle θ_p, and the position of the camera were taken into account. Our results indicate that the θ_p and q profiles can significantly affect the synchrotron radiation spot shape; it is simpler to record all synchrotron radiation if the camera is placed far from the plasma. An asymmetrical synchrotron radiation spot shape can be deduced when the effect of the drift orbit shift is taken into account. Our results can explain the asymmetrical ring-like synchrotron radiation spot shape from runaway electron beams in EAST experiments. © *2014 AIP Publishing LLC*. [http://dx.doi.org/10.1063/1.4881469]

I. INTRODUCTION

Runaway electrons can be a serious threat to the safe operation of tokamaks.[1,2] In particular, the energy of runaway electrons can reach as high as tens of MeV,[3–5] and even up to a maximum energy of 100 MeV in a tokamak like ITER.[6–8] To study the dynamics of those high-energy runaway electrons in experiments, it is critically important to diagnose the electron parameters effectively and correctly.

Monitoring of runaway electrons is typically done by measuring the thick-target bremsstrahlung emission or photoneutrons resulting by runaway electrons when they are lost and then impact the limiter or vessel structures. These data, however, can not provide information about the runaway electrons directly and are not suitable to detect high-energy runaway electron that are confined in the core of the plasma. In the case of large devices, it is much more difficult to obtain useful information from these methods, considering the high gamma and neutron background and shielding conditions.

Detection of the synchrotron radiation emitted by runaway electrons has been claimed as a way to diagnose high-energy runaway electrons directly in the core of the plasma.[3,4,9–12] The energy of runaway electrons can be deduced from their synchrotron radiation spectra, and information about the number of runaway electrons can be obtained from the synchrotron radiation intensity, which, in principle, can provide the runaway current. Moreover, the beam radius and pitch angle of the runaway electrons can be obtained from the shape of the synchrotron radiation spot of the electrons. Therefore, an understanding of the features of synchrotron radiation spectra and spot of runaway electrons affords a powerful tool to study runaway electrons in tokamaks. In experiments, detections of synchrotron radiation emitted by runaway electrons has been made by many devices.[5,7,13,14]

Recently, an investigation of asymmetrical ring-like runaway electron beams with energy above 30 MeV in EAST has been reported.[15] Similar observations have also been made in DIII-D recently.[5] In this paper, we carry out detailed analysis of the spectra of synchrotron radiation emitted by runaway electrons, and analyze the synchrotron radiation spot shapes for those EAST experiments. In Sec. II, we present the analysis of the synchrotron radiation spectra. In Sec. III, we discuss the analysis of the synchrotron radiation spot shape of runaway electrons in EAST. Our conclusions are summarized in Sec. IV.

II. SYNCHROTRON RADIATION SPECTRA

A. Asymptotic expressions of synchrotron radiation spectra

The motion of electrons in a tokamak plasma is a superposition of their guiding center motion that follows the helicity of the magnetic field lines, the cyclotron gyration motion around the guiding center with a frequency $\omega_{ce} = eB_0/m_e\gamma$, and the vertical centrifugal drift motion with velocity

$$v_{dr} = \left(v_\parallel^2 + \frac{1}{2}v_\perp^2\right)/(\omega_{ce}R_0) \approx v_\parallel^2/(\omega_{ce}R_0) \qquad (1)$$

due to curvature and gradient magnetic field drifts, in which γ is the relativistic factor. In tokamaks, the radiation of many runaway electrons is observed in the detector simultaneously. In this case, it is possible to introduce an averaged spectral density of the emitted power[10]

$$P_{full}(\lambda) = i\frac{ce^2}{\varepsilon_0\lambda^3\gamma^2}\left\{\int_C \frac{dy}{y}(1+2y^2)I_0(ay^3)\exp\left[\left(-\frac{3}{2}\xi\left(y-\frac{1}{3}y^3\right)\right]-\frac{4\eta}{1+\eta^2}\int_C dyyI_1(ay^3)\exp\left[-\frac{3}{2}\xi\left(y-\frac{1}{3}y^3\right)\right]\right\}, \quad (2)$$

where the integration path is taken along the line of steepest descent from a saddle point, R_0 is the major radius of magnetic surface, $I_{0,1}$ is the modified Bessel function, $a = \xi\eta/(1+\eta^2)$, $\xi = 4\pi R_0/3\lambda\gamma^3\sqrt{1+\eta^2}$, $\eta = v_\perp/v_{dr} \approx eB_0R_0\theta_p/m_ec\gamma$, with $\theta_p \approx \tan(\theta_p) = v_\perp/v_\parallel$ ($\theta_p \ll 1$), and θ_p is the pitch angle.

The integrands in Eq. (2) are highly oscillatory and the calculation of synchrotron spectra can become computationally intensive.[12] The asymptotic approximation of Eq. (2) can simplify the spectra analysis. Equation (2) can be easily integrated by the saddle point method, when

$$\xi = \frac{4\pi R_0}{3\lambda\gamma^3\sqrt{1+\eta^2}} \gg 1. \quad (3)$$

Two limit cases are possible.[10]

In the first case, the saddle point is $y_0 = (1,0)$, when

$$a = \xi\eta/(1+\eta^2) = \frac{4\pi R_0\eta}{3\lambda\gamma^3(1+\eta^2)^{3/2}} \lesssim 1. \quad (4)$$

The asymptotic expression of Eq. (2) will be

$$P_{as1}(\lambda) \approx \frac{ce^2}{4\varepsilon_0}\sqrt{\frac{2\sqrt{1+\eta^2}}{\lambda^5 R_0\gamma}}\left[I_0(a)+\frac{4\eta}{1+\eta^2}I_1(a)\right] \times \exp\left(-\frac{4\pi R_0}{3\lambda\gamma^3\sqrt{1+\eta^2}}\right). \quad (5)$$

Expression (5) has a maximum at $\lambda = \lambda_m$, with $\lambda_m \approx 8\pi R_0/15\gamma^3\sqrt{1+\eta^2}$. Then, $\xi = 2.5(\lambda_m/\lambda)$ can be obtained. The asymptotic expression can only describe correctly the features of the spectrum in the range $\lambda < \lambda_m$, where $\xi \gg 1$. Considering the limit from Eqs. (3) and (4), the value of $2.5/\eta(1+\eta^2)$ must be small, which implies that $2.5/\eta(1+\eta^2) \ll 1$. Therefore, the following extra condition:

$$\eta \gg 2 \quad \text{or} \quad \eta \ll 0.5 \quad (6)$$

must be also fulfilled to use Eq. (5) (P_{as1}). For EAST ($R_0 = 1.86$ m and $B_T = 2$ T), the parameter η may be written as

$$\eta = 1.116 \times 10^3\theta_p/E, \quad (7)$$

in which E is expressed in MeV.

In the second case, the saddle point is $y_0 = (\sqrt{1+\eta^2}/(1+\eta), 0)$, when

$$ay^3 = \frac{\xi\eta}{1+\eta^2}(\sqrt{1+\eta^2}/(1+\eta))^3 = \frac{4\pi R_0\eta}{3\lambda\gamma^3(1+\eta)^3} > 1. \quad (8)$$

The asymptotic expression of Eq. (2) becomes

$$P_{as2}(\lambda) \approx \frac{\sqrt{3}ce^2\gamma}{8\pi\varepsilon_0\lambda^2 R_0}\frac{(1+\eta)^2}{\sqrt{\eta}}\exp\left(-\frac{4\pi R_0}{3\lambda\gamma^3(1+\eta)}\right). \quad (9)$$

For expression (9), $\lambda_m \approx 2\pi R_0/3\gamma^3(1+\eta)$. Then, $ay^3 = 2[\eta/(1+\eta)^2](\lambda_m/\lambda)$ and $\xi = 2[(1+\eta)/\sqrt{1+\eta^2}](\lambda_m/\lambda)$. When $\eta \sim (1-2)$, Eq. (9) must be used instead of Eq. (5). The asymptotic expression correctly describes the features of the spectrum in the range $\lambda < \lambda_m$, where $ay^3 > 1$. In this case, inequality $\xi \gg 1$ holds automatically.

A comparison of the synchrotron radiation spectra of runaway electrons $P_{full}(\lambda)$ calculated numerically from Eq. (2) with asymptotic expressions P_{as1} (Eq. (5)) and P_{as2} (Eq. (9)) was presented in Ref. 16.

B. Bounds on the wavelength

Equations (3), (4), and (6) should be fulfilled to use Eq. (5) (P_{as1}), and Eqs. (3) and (8) should be fulfilled to use Eq. (9) (P_{as2}).[10,16] Therefore, we first deduce the validity conditions of P_{as1} and P_{as2} for EAST parameters.

Figure 1 (as in Ref. 12) shows the conditions required to ensure the validity of P_{as1} and P_{as2}, respectively, in typical EAST conditions, with $R_0 = 1.86$ m and $B_T = 2$ T. For the situation of P_{as1} shown in Figures 1(a) and 1(c), the wavelength range of application should be $\lambda_{lower} \lesssim \lambda \ll \lambda_{upper}$, in which λ_{lower} is marked by a blue line and λ_{upper} is marked by a black line. For the situation of P_{as2} shown in Figures 1(b) and 1(d), the wavelength range of application should be $\lambda < \lambda_{upper}$. The wavelength ranges that the infrared and visible light cameras can detect in EAST are also marked with dashed lines; red dashed lines correspond to the infrared camera ((3–8) μm) and green dashed lines correspond to the visible light camera ((0.38–0.75) μm).

In Figures 1(a) and 1(b), the validity conditions of P_{as1} and P_{as2} for a runaway energy $E = 40$ MeV and pitch angles ranging from $\theta_p = 0$–0.2 are shown. In Figures 1(c) and 1(d), the data for a pitch angle of $\theta_p = 0.1$ and a runaway energy of $E = 20$–50 MeV are shown. These data indicate that the asymptotic expression P_{as1} is not valid when the visible light camera is used in EAST. P_{as2} should be used when $\theta_p < 0.15$.

As for infrared camera, it seems that we can use P_{as1} when $\theta_p < 0.1$. However, for P_{as1}, the validity condition is uncertain when we use the inequality $\lambda \ll \lambda_{upper}$. In this case, it is necessary to consider Eqs. (6) and (7) as the supplementary restraints. For P_{as1} from Eqs. (6) and (7), the following inequalities (validity conditions) may be obtained:

$$\theta_p \ll 0.02 \quad \text{or} \quad \theta_p \gg 0.1 \quad (\text{Fig.1a}, E = 40\,\text{MeV}), \quad (10)$$

$$E \gg 200\,\text{MeV} \quad \text{or} \quad E \ll 50\,\text{MeV} \quad (\text{Fig.1c}, \theta_p = 0.1). \quad (11)$$

For example, for runaway parameters $E = 30$ MeV, $\theta_p = 0.1$, and $\lambda = 5$ μm one can obtain values of $\eta = 3.7$ and $\xi \approx 1.9$; these values are outside of valid conditions. Therefore, it is not valid to use P_{as1} in typical EAST conditions.

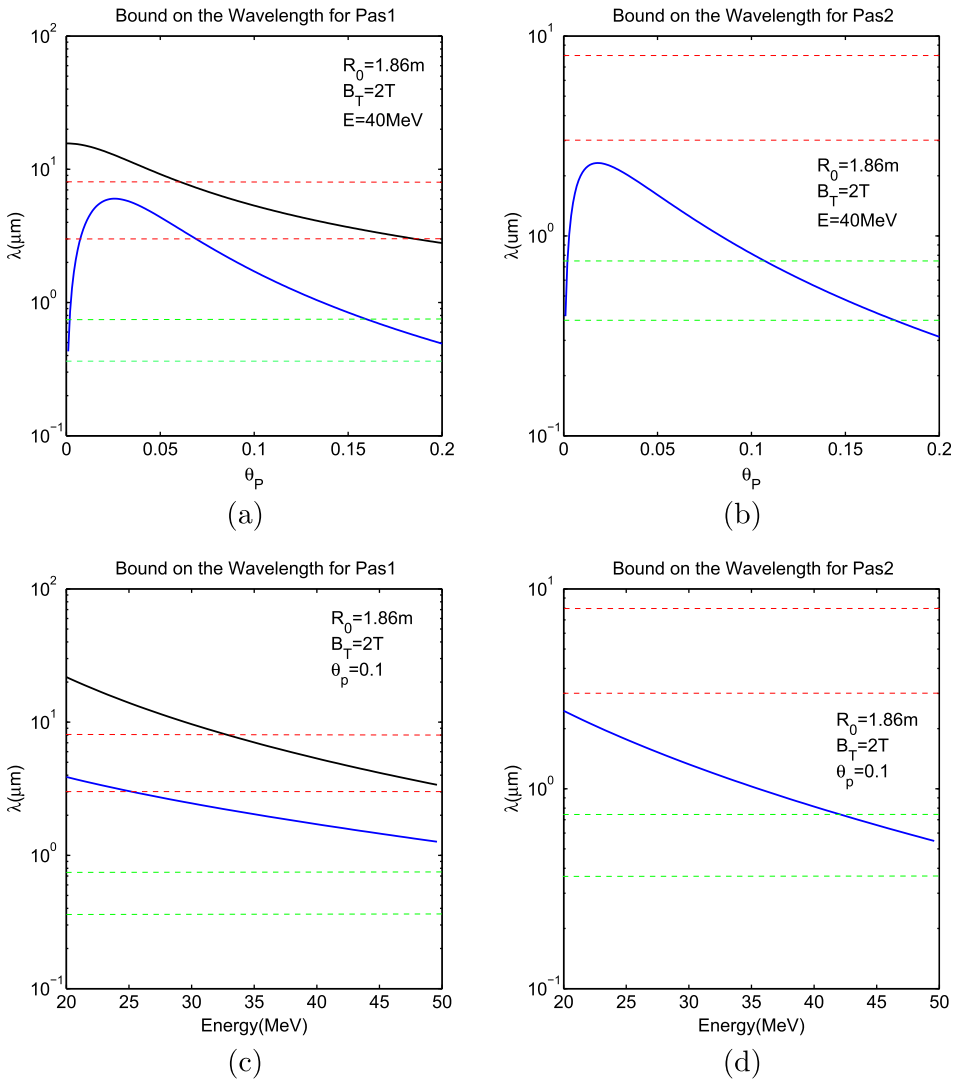

FIG. 1. Condition required for the validity of P_{as1} and P_{as2}, respectively, in EAST with $R_0 = 1.86$ m and $B_T = 2$ T. The case of P_{as1} is shown in panels (a) and (c) in which the wavelength range of application should be $\lambda_{lower} \lesssim \lambda \ll \lambda_{upper}$. The case of P_{as2} is shown in panels (b) and (d) in which the wavelength range of application should be $\lambda < \lambda_{upper}$. The wavelength ranges that can be detected by infrared and visible light cameras in EAST are also marked with dashed lines. A fixed energy, $E = 40$ MeV, was used in (a) and (b), and a fixed pitch angle, $\theta_p = 0.1$ was used in (c) and (d).

Although the validity condition is sensitive to the wavelength, P_{as2} can be used for a wide range of plasma parameters in EAST when the visible light camera is used. The usability of P_{as2} is not sensitive to wavelength, which is a beneficial attribute when a camera with a wide wavelength range is used to detect the synchrotron radiation spectra.

C. Synchrotron radiation spectra in EAST

In Ref. 15, the experimental investigation of asymmetrical ring-like runaway electron beams in EAST has been reported. The asymptotic expression P_{as1} was used to calculate the synchrotron radiation spectra during this experiment. In the present paper, we re-calculate the spectra based on P_{as2}, which is more suitable than P_{as1} for EAST. The results are shown in Figure 2. The wavelength range of the visible light camera ((0.38–0.75) μm) is in the range $\lambda < \lambda_m$, which ensures that the asymptotic expression P_{as2} represents the spectra correctly.

In Ref. 15, in which calculations were based on P_{as1}, it has claimed that "in order for synchrotron radiation to emit in the visible light range, the runaway electrons must attain an energy of at least 40 MeV when their pitch angles are small ($\theta_p = 0.05$). However, this study found that for runaway electrons with large pitch angles ($\theta_p = 0.15$), 30 MeV is a sufficient energy." Using the result in Figure 2, in which the calculations were based on P_{as2}, still for runaway electrons with large pitch angles ($\theta_p = 0.15$), 30 MeV will be enough

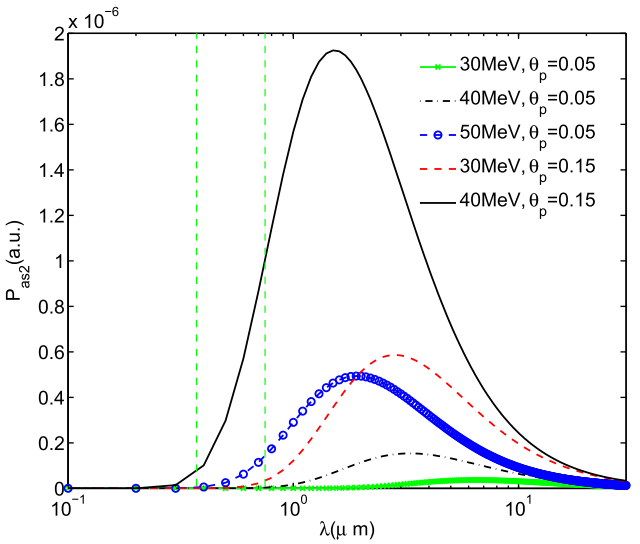

FIG. 2. Synchrotron radiation spectra in EAST with $R_0 = 1.86$ m, $B_T = 2$ T for expected values of E and θ_p. The wavelength range for the visible light camera ((0.38–0.75) μm) is marked with green dashed lines.

energy to emit synchrotron radiation in the visible range. However, for electrons with $\theta_p = 0.05$ and $E = 40\,\text{MeV}$, it seems that only a tiny part of the synchrotron radiation falls into the visible range. For electrons with $\theta_p = 0.05$, $E = 50\,\text{MeV}$, large part of the synchrotron radiation falls into the visible range. Therefore, it is more accurate to state that "To emit synchrotron radiation in the range of visible wavelengths in EAST, runaway electrons must attain an energy greater than 50 MeV when their pitch angles are small ($\theta_p = 0.05$)." It must be noted this re-calculated result does not affect conclusions of the investigation about asymmetrical ring-like runaway electron beams in Ref. 15.

III. SYNCHROTRON RADIATION SPOT SHAPE

The analysis of the shape of the synchrotron radiation spot in the tokamak is another important part of the spectrum analysis, which can provided detailed information about the pitch angle of the runaway electron, the shape of the runaway beam, etc.[3,14] We have written a code to calculate the shape of the synchrotron radiation spot emitted by runaway electrons in a toroidal geometry detected by a visible light camera in EAST, in which the safety factor $q(r)$, the horizontal displacement of the electron drift surfaces with respect to the corresponding magnetic surfaces, the pitch angle θ_p, and the position of the camera were all taken into account.

A. Analytical expressions

The analytical treatment of the calculation of the synchrotron radiation spot shape from runaway electrons has been carried out in Ref. 9. The coordinates we used in the calculation are shown in Figure 3, in which several magnetic surfaces (marked in red) and a drift orbit surface of runaway electrons (marked in blue) are shown. The transverse cross sections of the magnetic surfaces are assumed to be nearly circular, and the displacements of the magnetic surfaces relative to each other are neglected. In this case the major radius of the magnetic surfaces R_0 will have the form $R_0 \to R_m$. θ and φ are the poloidal and toroidal angles, respectively. In Figure 3, r and r_e represent the radius of the magnetic surface and the radius of the drift orbit surface, respectively, and δ_e represents orbit shift between magnetic and drift surfaces

$$r = \sqrt{r_e^2 - \delta_e^2 \sin^2\theta} - \delta_e \cos\theta. \tag{12}$$

The value δ_e is given by $\delta_e = q\gamma m_e c/eB_0$.[17,18] Runaway electrons in different magnetic surfaces with different $q(r)$ values will have different orbit shifts.

The position of the visible light camera in EAST in Cartesian coordinates has the form

$$\mathbf{Q}_{det} = D\mathbf{e}_x + Y_{det}\mathbf{e}_y + Z_{det}\mathbf{e}_z, \tag{13}$$

where $D = 148\,\text{cm}$, $Y_{det} = 185\,\text{cm}$, and $Z_{det} = 0$, which is close to the plasma and viewing tangentially into the plasma from the equatorial plane. In EAST case, the magnetic field is directed toward the detector. Schematic of the relative positions of the beam of runaway electrons and the camera is shown in Figure 4.

The synchrotron radiation emitted along the runaway electron velocity vector falls into the camera when the following conditions are satisfied:[9]

$$\sin\Delta \approx -\frac{r\sin\theta}{q(r)R_m} + \frac{v_\perp \cos(\theta-\alpha)}{v_\parallel} + \frac{Y_{det} - R_m + r\cos\theta}{D}, \tag{14}$$

$$Z_{det} - r\sin\theta \approx \left[\frac{r\cos\theta}{q(r)R_m} + \frac{v_\perp \sin(\theta-\alpha)}{v_\parallel} + \frac{v_{dr}+v_v}{v_\parallel}\right] \times [D + (R_m - r\cos\theta)\sin\Delta], \tag{15}$$

in which $|\Delta| \ll 1$ is the range of toroidal angles over which the synchrotron radiation can be recorded by the camera ($\varphi = \pi/2 + \Delta$). Then, $[D + (R_m - r\cos\theta)\sin\Delta]$ represents the distance from the camera to the plane that the runaway electrons cross, which is perpendicular to the x-axis. The velocity v_v is determined by the vertical magnetic field $\mathbf{B}_V$. α is the cyclotron gyration phase with $\dot{\alpha} \approx -\omega_{ce}$.

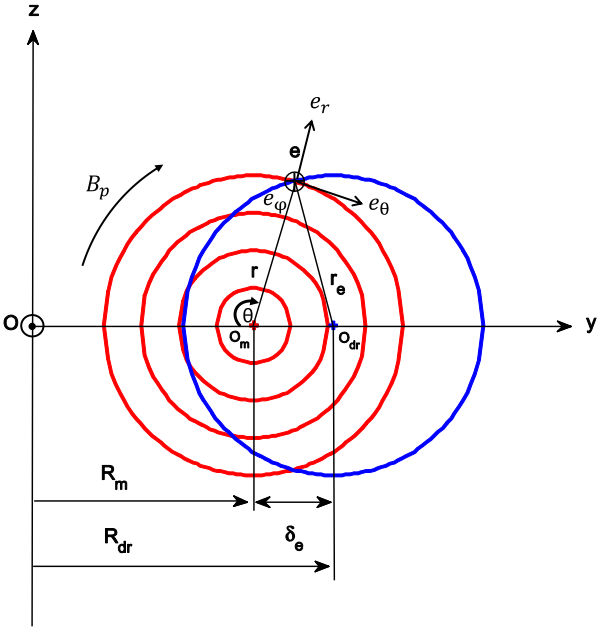

FIG. 3. System of coordinates used in the calculations. Magnetic surfaces are marked in red and the drift orbit surface of the runaway electrons is marked in blue. The direction of the poloidal magnetic field is shown and the component of the toroidal magnetic field is negative, with $\mathbf{B}_T = -B_\varphi \mathbf{e}_\varphi$.

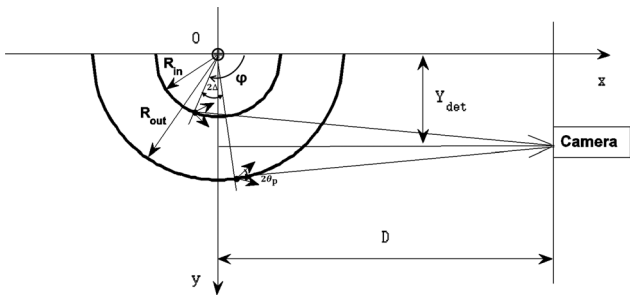

FIG. 4. Schematic of the relative positions of runaway electrons beam and the camera in the plane $z = 0$. R_{in} and R_{out} are the inner and outer major radius of the beam. The cross sections (through this plane) of the cones of radiation emitted by runaway electrons are represented schematically, with vertex angle $2\theta_p$.

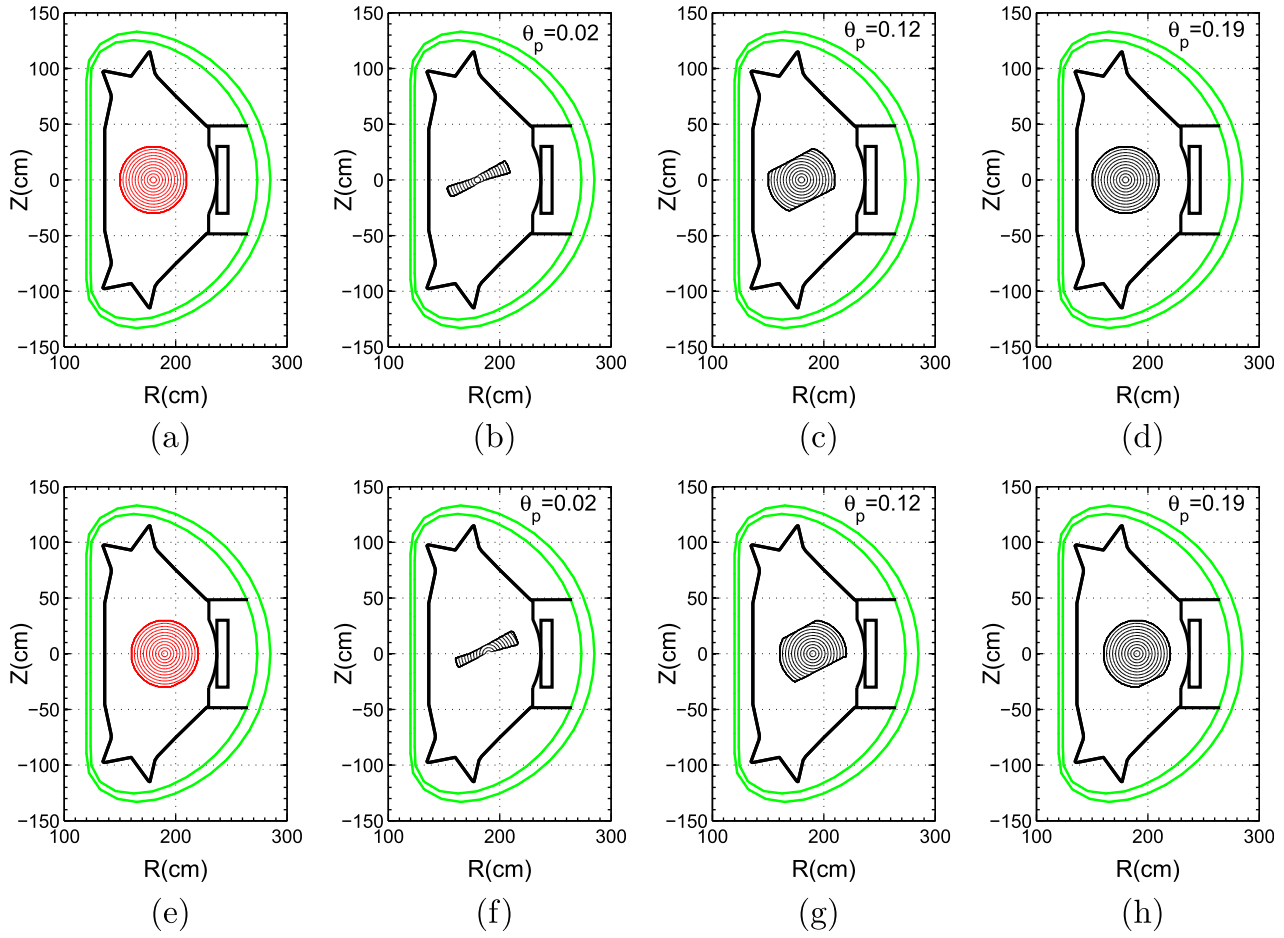

FIG. 5. Results of synchrotron radiation spot shape for runaway electrons with energy $E = 30\,\mathrm{MeV}$, $r \in [0, 30]\,\mathrm{cm}$, and $q = 2$. Electron orbits without considering orbit shift is shown in panel (a) in red, the resulting synchrotron radiation spot for three pitch angles are shown in panel (b)–(d) in black. Electron orbits considering orbit shift ($\delta_e \approx 10\,\mathrm{cm}$) is shown in panel (e) in red, the resulting synchrotron radiation spot for three pitch angles are shown in panel (f)–(h) in black.

B. Calculation considering drift orbit shift

At first, we consider the model that is closed to the experimental situation in EAST and compare the calculation results with and without considering the large drift orbit shift of high energy runaway electrons. The results are shown in Figure 5. Figure 5(a) shows the electron orbits without considering orbit shift with $r = r_e \in [0, 30]\,\mathrm{cm}$, and Figures 5(b)–5(d) show the calculated synchrotron radiation spot for different pitch angles without considering orbit shift. Figure 5(e) shows the electron orbits considering orbit shift with $r \in [0, 30]\,\mathrm{cm}$ and δ_e is determined by $\delta_e = q\gamma m_e c/eB_0$, and Figures 5(f)–5(h) highlight the calculated synchrotron radiation spot for different pitch angles considering orbit shift.

The synchrotron spot shows an inclination with respect to the equator, which is related to the q profile of the plasma and will be discussed below. In the model calculations, the q value was taken to be $q = 2$, i.e., not changing with respect to the plasma radius.

Based on the results that did not consider orbit shift, the shape of the synchrotron radiation spot is strongly dependent on the pitch angle θ_p of the runaway electrons. When θ_p is small, as in Figure 5(b), only the synchrotron radiation from a small fraction of runaway electrons beam can be recorded by the camera, which results in a narrow pattern. This finding is a consequence of the fact that the synchrotron radiation is emitted in a narrow cone with an aperture of about $1/\gamma$ in the direction parallel to its velocity vector due to relativistic effects.[19] The aperture of the cone will be about $(2\theta_p + 1/\gamma \approx 2\theta_p)$ with respect to the direction of the guiding center motion, which should be the direction of the magnetic field. The vertical height of the synchrotron radiation spot with respect to the inclination of the spot will increase if the pitch angle θ_p increases, as can be seen in Figure 5(c). Finally, to record all of the synchrotron radiation from a runaway electron beam, a larger value of θ_p is needed, which can be seen in Figure 5(d).

For the situation when orbit shift is taken into account and the upper edge of the runaway beam can be recorded in the camera in typical EAST experiments, the following condition must be satisfied:[9]

$$\theta_p \geq \frac{r_{beam}}{D_{top}} + \frac{\delta_{beam} - r_{beam}\Delta\theta}{qR_0}, \tag{16}$$

where

$$D_{top} \approx D - (R_0 + \delta_{beam}) \times \left[\frac{R_0 + \delta_{beam} - Y_{det} - r_{beam}\Delta\theta}{D} - \frac{r_{beam}}{qR_0}\right], \tag{17}$$

in which $\Delta\theta$ represents the range of poloidal angle in the vicinity of upper edge of the runaway beam ($\theta = \theta_{upper} + \Delta\theta$), where $\tan\theta_{upper} = -r_{beam}/\delta_{beam}$. In the EAST experimental situation, these equations yield $\theta_p \gtrsim 0.20$ if $|\Delta\theta| \sim 0.1$, with $\delta_{beam} = \delta_e \approx 10\,\text{cm}$, which can be confirmed approximately in Figure 5(h). The larger the value of D, the smaller θ_p value that is required. Therefore, it will be easier to record all of the synchrotron radiation if the camera is placed far from the plasma.

C. Effect of the *q* profile on synchrotron spot shape

We have discussed that the radiation spot shows an inclination with respect to the equator, particularly when θ_p is very small, which is related to the q profile of the plasma. We can understand from Eq. (15) that when θ_p is very small, which gives $-r\sin\theta \approx Dr\cos\theta/q(r)R_m$. Then, one cans obtain[9]

$$\tan(\beta_{inc}) = -\tan\theta \approx \frac{D}{q(r)R_m}, \tag{18}$$

in which β_{inc} represents the angle in the poloidal plane between the equator and a line in the direction of the inclination, as shown in Figure 6(e).

To analyze the effect of the q profile on the synchrotron radiation spot shape, we show the results of synchrotron spots assuming several different q profiles in Figure 6. If the value of q does not depend on plasma radius, as in Figures 6(a) and 6(b), the angle β_{inc} is independent of the plasma radius. A larger q value corresponds to a smaller β_{inc} value, which can also be deduced from Eq. (18). For the q profiles in Figures 6(c) and 6(d), we obtain curving synchrotron spot shapes because β_{inc} changes with respect to the plasma radius in these cases.

It can be seen, the q profile can affect the synchrotron radiation spot shape of the runaway electrons. It must be stressed that this case is applicable when all runaway electrons have identical energies and pitch angles. In a more realistic case, the energies and pitch angles of runaway electrons are not identical and instead tend to be characterized by distributions. In this case, more complicated analysis is needed.

D. Effect of orbit shift on synchrotron spot shape

The effect of drift orbit shift on synchrotron spot shape can be seen clearly in the case of a hollow ring-like runaway electron beam. This case assumes that the radius of the drift orbit is almost constant as the runaway electron energy and orbit shift increase.[20–22] Note, a hollow synchrotron spot does necessarily mean a hollow runaway electron beam cross-section (see Eqs. (14) and (15)), see also Ref. 14. But a hollow runaway electron beam cross-section does not necessarily mean an apparently hollow synchrotron spot.

An example is shown in Figure 7, in which we consider a runaway electron beam with an energy $E = 30\,\text{MeV}$, $\theta_p = 0.12$, and $r \in [15, 30]\,\text{cm}$. Here, q profile used is shown in Figure 6(d). In the case that drift orbit shift is not taken into account (as shown in Figure 7(b)), we obtain a symmetrical hollow ring-like synchrotron spot shape. The radius of the synchrotron spot is determined by the size of the runaway

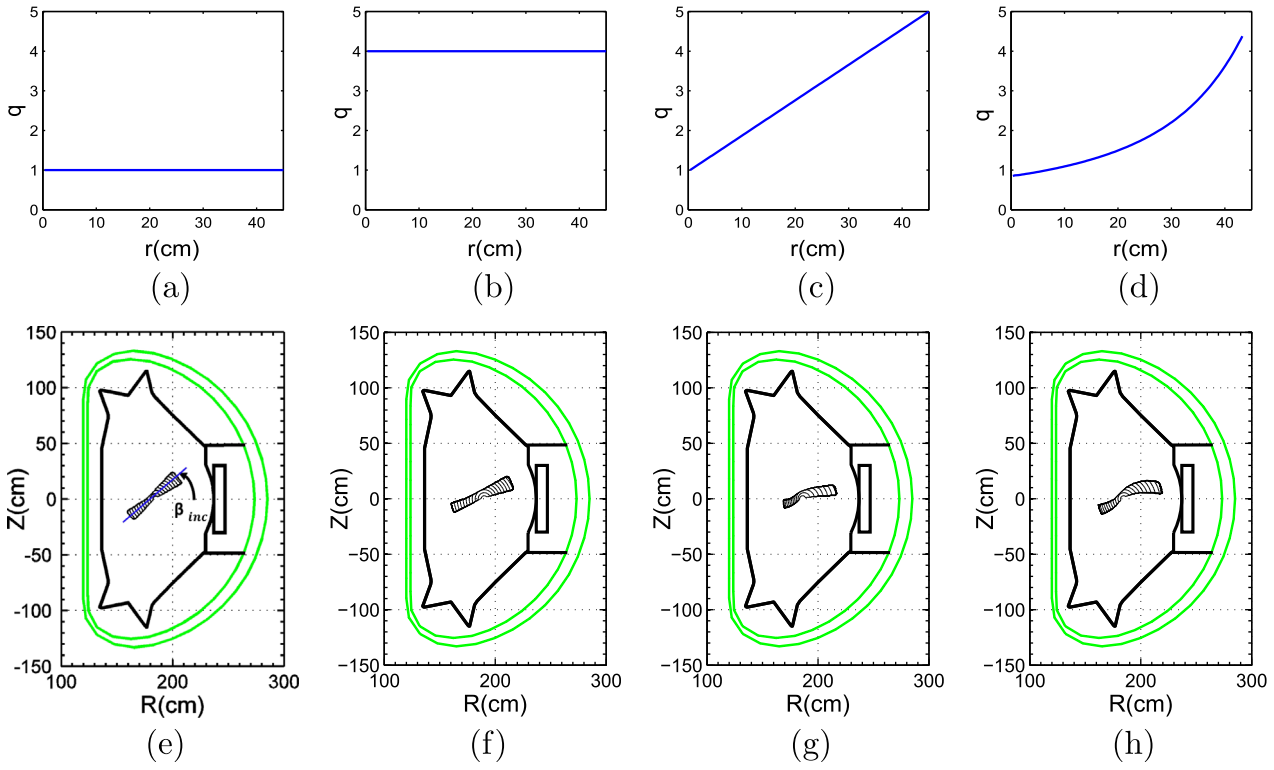

FIG. 6. Results of synchrotron radiation spot shape assuming different q profiles. Drift orbit shift is taken into account, with an energy $E = 30\,\text{MeV}$ and pitch angle $\theta_p = 0.02$ for all cases.

electron beam; the vertical height of the synchrotron spot with respect to inclination is determined by the value of θ_p.

However, in the case that drift orbit shift is taken into account (as shown in Figure 7(d)), asymmetrical hollow ring-like synchrotron spot shape is obtained in which the synchrotron radiation of runaway electrons in the lower low field side can not be recorded by the camera. This inability to record is related to the size of the electron beam and the value of the orbit shift. When we consider a large orbit shift of runaway electrons, the radius of their drift orbit surface r_e will be different from the radius of the magnetic surface r (see Eq. (12)). For runaway electrons in the same drift orbit surface, electrons in the lower low field side will be located on a magnetic surface with a larger radius than electrons in the upper high field side. For example, for electrons with $r_e = 25\,\text{cm}$ and $\delta_e = 9\,\text{cm}$, one obtains $r \approx 17.8\,\text{cm}$ for electrons with $\theta = \pi/4$ and $r \approx 30.5\,\text{cm}$ for electrons with $\theta = 5\pi/4$. For certain values of D and θ_p, the detectability limit of the synchrotron radiation is determined by r and θ, not r_e (see Eqs. (14) and (15)). The synchrotron radiation in the lower low field side can not be detected when the orbit shift of runaway electrons are large enough. This is why we recover an asymmetrical synchrotron spot when drift orbit shift is taken into account.

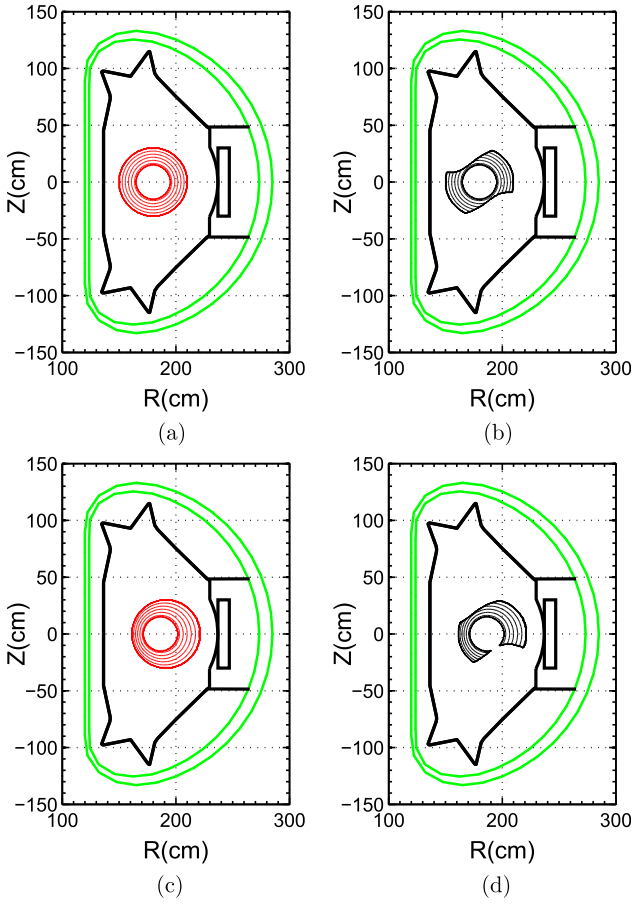

FIG. 7. Results of synchrotron spot shape for runaway electrons with energy $E = 30\,\text{MeV}$, $\theta_p = 0.12$, and $r \in [15, 30]\,\text{cm}$. Electron orbits without considering orbit shift is shown in panel (a) in red, the resulting synchrotron spot is shown in panel (b) in black. Electron orbits considering orbit shift is shown in panel (c) in red, the resulting synchrotron spot is shown in panel (d) in black.

E. Asymmetrical synchrotron spot in EAST experiments

In the EAST experiments, asymmetrical ring-like synchrotron radiation spots from the runaway electron beams have been observed with the visible light camera.[15] A runaway discharge is shown in Figure 8. The discharge was an ohmic discharge and was performed in the limiter configuration. Runaway electrons were created during the start-up phase of the discharge by the ohmic coil, which strongly affected the electron cyclotron emission (ECE) signals, and were maintained for the whole duration of the discharge. The bulk electron temperature is obtained from a soft x-ray pulse height analysis (PHA) system. At the plasma center, it is only about $T_e \approx 0.55\,\text{keV}$ during the plasma current flat-top phase. The inductive electric field is about $E_{\|} = V_p/2\pi R_0 \approx 0.1\,\text{V/m}$, and effective charge number of ions is about $Z_{eff} \approx 3$. In this case, considering the effect of acceleration by electric field, the collisions with plasma particles and the synchrotron radiation losses, runaway electrons can be accelerated up to 40 MeV in the flat-top phase of discharge. High energy runaway electrons in plasma can carry considerable current. It will affect the q profile of plasma. However, we can not obtain this q profile or current profile accurately in experiments in EAST. In this case q profile that shown in Figure 6(d) will be used in the following calculations as an assumption.

One frame of the images from the visible light camera (at 3.81 s) is shown in Figure 9(a). The intensity of the synchrotron radiation in lower low field side is barely visible. The runaway beam is located around the $q = 2$ rational surface. An average orbit shift of about $\langle \delta_e \rangle \approx 8.6\,\text{cm}$ can be deduced based on the geometry of the frame. Therefore, based on relation $\delta_e = q\gamma m_e c/eB_0$, the energy of these runaway electrons can be deduced to be roughly 26 MeV. In this energy range, the pitch angle of those runaway electrons

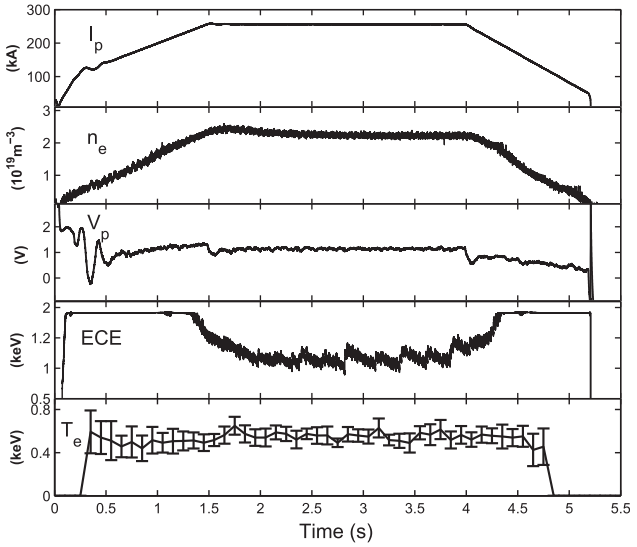

FIG. 8. Time slice of a runaway discharge in the EAST tokamak. The waveforms are plasma current, line-averaged density, loop voltage, ECE, and electron temperature at the plasma centre obtained from the soft x-ray PHA system.

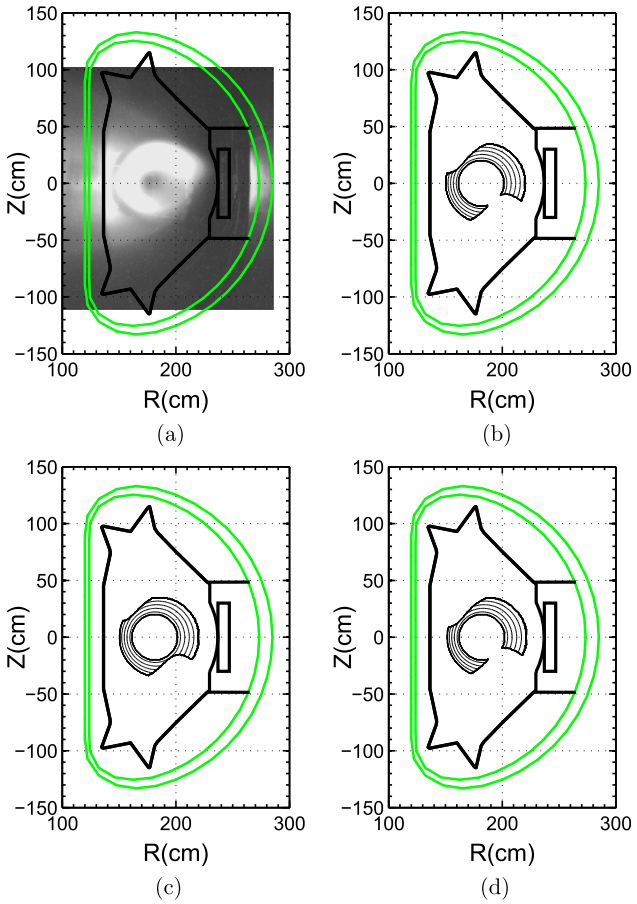

FIG. 9. Asymmetrical ring-like synchrotron radiation spot from the runaway electron beam in EAST. (a) One frame of the images from the visible light camera at 3.81 s. (b) Calculated synchrotron radiation spot shape considering the orbit shift, for electrons with energy $E = 26$ MeV, pitch angle $\theta_p = 0.16$, and $r \in [20, 35]$ cm.(c) Calculation with energy $E = 26$ MeV, pitch angle $\theta_p = 0.18$, and $r \in [20, 35]$ cm.(d) Calculation with energy $E = 30$ MeV, pitch angle $\theta_p = 0.16$, and $r \in [20, 35]$ cm.

must be large enough so that we observe synchrotron radiation at visible wavelengths.

In Figure 9(b), we show the results of the synchrotron radiation spot shape considering the orbit shift for runaway electrons with energy $E = 26$ MeV, $r \in [20, 35]$ cm, and pitch angle $\theta_p = 0.16$. As can be seen in Figure 9(b), asymmetrical synchrotron spot is deduced due to the effect of orbit shift. The result of the calculations and the experimental results agree approximately with each other. However, considering the synchrotron radiation spectra in this case (as shown in Figure 10), the synchrotron radiation is barely visible for runaway electrons with $E = 26$ MeV and $\theta_p = 0.16$.

Calculations for runaway electrons with energy $E = 26$ MeV and pitch angle $\theta_p = 0.18$ are shown in Figure 9(c). Likewise, calculations for runaway electrons with energy $E = 30$ MeV and pitch angle $\theta_p = 0.16$ are given in Figure 9(d). We see that the shape of the synchrotron radiation spot is much more sensitive to the pitch angle than the energy of the runaway electrons. Case in Figure 9(d), $E = 30$ MeV and $\theta_p = 0.16$, can meet the requirement of both the synchrotron radiation spectra and synchrotron radiation spot shape.

Another frame of the images from the visible light camera (at 1.93 s) is shown in Figure 11(a). Average value of q

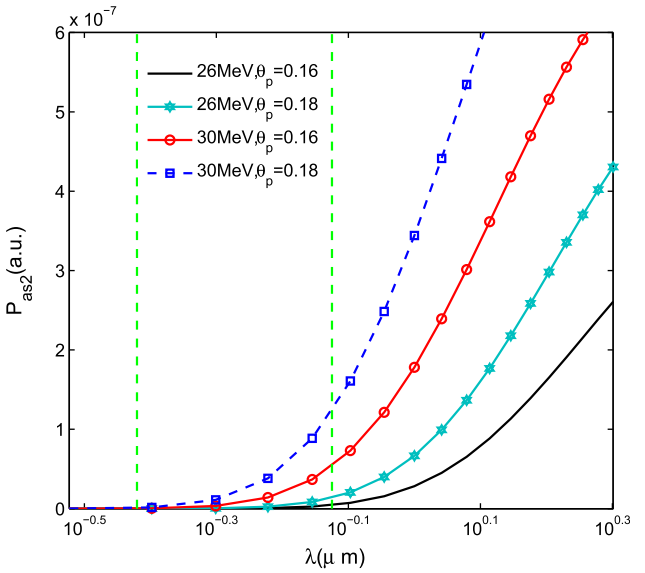

FIG. 10. Synchrotron radiation spectra for four expected values of E and θ_p. The wavelength range for the visible light camera ((0.38–0.75) μm) is marked with green dashed lines.

(with $\langle q \rangle = 1.2$), where this very narrow ring-like runaway beam located, was used in the calculation. The calculation results are presented in Figure 11(b). It indicates runaway electrons with energy $E = 30$ MeV, pitch angle $\theta_p = 0.16$, and $r \in [22, 30]$ cm can answer for the synchrotron spot shown in Figure 11(a).

The calculated synchrotron radiation spectra and spot shape supplement each other. Both the beam radius and the pitch angle of the runaway electrons can be obtained from the calculated synchrotron radiation spot shape. Then, the energy of the runaway electrons can be deduced by using the calculated synchrotron spectra in combination. However, there are still some differences in the detailed spot shape and inclination between the experimental image and the calculated results. It might be because we have used monoenergetic runaway electrons with the same pitch angles in the calculations. Distributions of those parameters in experiments will be more complicated than what we have used.

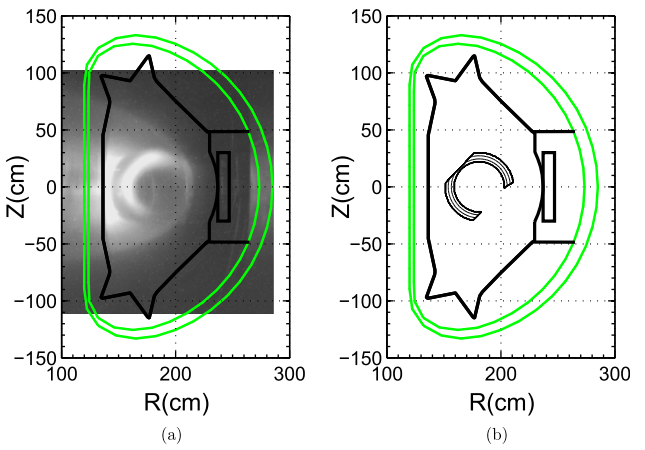

FIG. 11. Asymmetrical ring-like synchrotron radiation spot from the runaway electron beam in EAST. (a) One frame of the images from the visible light camera at 1.93 s. (b) Calculated synchrotron radiation spot shape considering the orbit shift, for electrons with energy $E = 30$ MeV, pitch angle $\theta_p = 0.16$, and $r \in [22, 30]$ cm.

Theoretical results have indicated recently that the diffusion coefficient for runaway electron near the rational drift surface due to magnetic perturbations can be very low. It can expect this effect may lead to the formation of the nested beams of runaway electrons.[23] It can be one possibility to explain the formation of ring-like runaway beam in EAST experiments. Further research is needed to understand this phenomenon.

IV. CONCLUSIONS

We have presented a detailed analysis of the spectra of synchrotron radiation emitted by runaway electrons, and an analysis of synchrotron radiation spot shape in EAST.

To analyze the synchrotron radiation spectra correctly for the interpretation of the EAST experiments, bounds on the wavelength for asymptotic expressions P_{as1} and P_{as2} have been considered. The conditions that are required to ensure validity of those asymptotic expressions for the EAST experiments have been found. The correct synchrotron radiation spectra for typical EAST runaway parameters are presented.

We developed a code to calculate the shape of the synchrotron radiation spot emitted by runaway electrons in a toroidal geometry that was detected by the visible light camera in EAST. The safety factor $q(r)$, the horizontal displacement of electron drift surfaces with respect to magnetic surfaces δ_e, the pitch angle θ_p, and the position of the camera were taken into account. The results indicate that, synchrotron radiation spots show an inclination with respect to the equator, which is related to the q profile of the plasma, and the vertical height of the synchrotron radiation spot with respect to the inclination of the spot determined by θ_p. It is easier to record all of the synchrotron radiation if the camera is placed far from the plasma.

The influence of large drift orbit shift of high energy runaways on the camera record possibility is the main reason why an asymmetrical synchrotron radiation spot can be observed in tokamak experiments. Calculations of synchrotron radiation spot shape from runaway electrons agree approximately with EAST experimental results when asymmetrical ring-like synchrotron radiation spots ware observed with the visible light camera.

ACKNOWLEDGMENTS

This work was supported by the JSPS-NRF-NSFC A3 Foresight Program in the field of Plasma Physics (NSFC No. 11261140328) partially, by the National Nature Science Foundation of China through Grant No. 11205197 and was partially supported by the CAS Key International S&T Cooperation Project collaboration with Grant No. GJHZ1123.

[1]S. Mirnov, J. Wesley, N. Fujisawa, Y. Gribov, O. Gruber, T. Hender, N. Ivanov, S. Jardin, J. Lister, and F. Perkins, Nucl. Fusion **39**, 2251 (1999).
[2]T. Hender, J. Wesley, J. Bialek, A. Bondeson, A. Boozer, R. Buttery, A. Garofalo, T. Goodman, R. Granetz, and Y. Gribov, Nucl. Fusion **47**, S128 (2007).
[3]K. Finken, J. Watkins, D. Rusbldt, W. Corbett, K. Dippel, D. Goebel, and R. Moyer, Nucl. Fusion **30**, 859 (1990).
[4]I. Pankratov, R. Jaspers, K. Finken, I. Entrop, and G. Mank, Nucl. Fusion **38**, 279 (1998).
[5]J. H. Yu, E. M. Hollmann, N. Commaux, N. W. Eidietis, D. A. Humphreys, A. N. James, T. C. Jernigan, and R. A. Moyer, Phys. Plasmas **20**, 042113 (2013).
[6]M. Bakhtiari, G. Kramer, M. Takechi, H. Tamai, Y. Miura, Y. Kusama, and Y. Kamada, Phys. Rev. Lett. **94**, 215003 (2005).
[7]R. Jaspers, N. J. L. Cardozo, F. C. Schuller, K. H. Finken, T. Grewe, and G. Mank, Nucl. Fusion **36**, 367 (1996).
[8]G. Papp, M. Drevlak, T. Fulop, P. Helander, and G. I. Pokol, Plasma Phys. Controlled Fusion **53**, 095004 (2011).
[9]I. Pankratov, Plasma Phys. Rep. **22**, 535 (1996).
[10]I. Pankratov, Plasma Phys. Rep. **25**, 145 (1999).
[11]R. Jaspers, N. Lopes Cardozo, A. Donne, H. Widdershoven, and K. Finken, Rev. Sci. Instrum. **72**, 466 (2001).
[12]A. Stahl, M. Landreman, G. Papp, E. Hollmann, and T. Fulop, Phys. Plasmas **20**, 093302 (2013).
[13]R. Jaspers, K. H. Finken, G. Mank, F. Hoenen, J. A. Boedo, N. J. L. Cardozo, and F. C. Schuller, Nucl. Fusion **33**, 1775 (1993).
[14]I. Entrop, R. Jaspers, N. J. L. Cardozo, and K. H. Finken, Plasma Phys. Controlled Fusion **41**, 377 (1999).
[15]R. J. Zhou, L. Q. Hu, E. Z. Li, M. Xu, G. Q. Zhong, L. Q. Xu, S. Y. Lin, J. Z. Zhang, and T. E. Team, Plasma Phys. Controlled Fusion **55**, 055006 (2013).
[16]I. Pankratov, I. Pavlenko, and O. Pomazan, J. Kharkiv National University (series "Nuclei, Particles, Fields") **1059**, 39 (2013). See www-nuclear.univer.kharkov.ua/engl/fs.htm.
[17]R. Jaspers, N. J. L. Cardozo, K. H. Finken, B. C. Schokker, G. Mank, G. Fuchs, and F. C. Schuller, Phys. Rev. Lett. **72**, 4093 (1994).
[18]X. Y. Guan, H. Qin, and N. J. Fisch, Phys. Plasmas **17**, 092502 (2010).
[19]G. Bekefi, *Radiation Processes in Plasmas*, Wiley Series in Plasma Physics (Wiley, New York, 1966), Vol. 1.
[20]S. J. Zweben, B. V. Waddell, D. W. Swain, and H. H. Fleischmann, Nucl. Fusion **20**, 477 (1980).
[21]M. deRover, N. J. L. Cardozo, and A. Montvai, Phys. Plasmas **3**, 4478 (1996).
[22]M. deRover, N. J. L. Cardozo, and A. Montvai, Phys. Plasmas **3**, 4468 (1996).
[23]S. Abdullaev, K. Finken, and M. Forster, Phys. Plasmas **19**, 072502 (2012).